

Non-Hermitian Topological Phase Transition of the Bosonic Kitaev Chain

Clément Fortin¹, Kai Wang¹, and T. Pereg-Barnea¹

¹*Department of Physics, McGill University, Montréal, Québec, Canada H3A 2T8*

(Dated: December 16, 2024)

The bosonic Kitaev chain, just like its fermionic counterpart, has extraordinary properties. For example, it displays the non-Hermitian skin effect even without dissipation when the system is Hermitian. This means that all eigenmodes are exponentially localized to the edges of the chain. This is possible since the \hat{x} and \hat{p} quadratures decouple such that each of them is governed by a non-Hermitian dynamical matrix. In the topological phase of the model, the modes conspire to lead to exponential amplification of coherent light that depends on its phase and direction. In this work, we study the robustness of this topological amplification to on-site dissipation. We look at uniform and non-uniform dissipation and study the effect of different configurations. We find remarkable resilience to dissipation in some configurations, while in others the dissipation causes a topological phase transition which eliminates the exponential amplification. For example, when the dissipation is placed on every other site, the system remains topological even for very large dissipation which exceeds the system's non-Hermitian gap and the exponential amplification persists. On the other hand, dividing the chain into unit cells of an odd number of sites and placing dissipation on the first site leads to a topological phase transition at some critical value of the dissipation. Our work thus provides insights into topological amplification of multiband systems and sets explicit limits on the bosonic Kitaev chain's ability to act as a multimode quantum sensor.

I. INTRODUCTION

Topological systems represent natural frameworks to investigate quantum sensing protocols, where one requires the sensor to display high sensitivity to specific perturbations while being robust to other common perturbations. Among these topological systems are bosonic quadratic Hamiltonians. These differ fundamentally from their fermionic counterpart, in that a Hermitian Hamiltonian can give rise to non-Hermitian (NH) dynamics [1–4]. They are also standard platforms for studying magnons [5, 6] and the quadrature squeezing of light [7, 8]—notably used to enhance gravitational wave sensitivity [9–11] and perform quantum computations [12].

Features unique to NH systems, such as exceptional points [13–24] or the non-Hermitian skin effect [25–30] have recently been proposed as resources for enhanced sensitivity in the context of quantum sensing. Perhaps most promising is nonreciprocal transport [31], which is tightly linked to directional amplifiers [32, 33] and has the advantage of not requiring fine parameter tuning (as is the case for exceptional-point-based sensing) or high intracavity photon number and reflection gain [34]. It can be realized via reservoir engineering [35–37], Josephson circuits [38–40] and optomechanical systems [41–46].

In the bosonic Kitaev chain (BKC) [2, 47], nonreciprocity caused by nearest-neighbor squeezing leads the system to be highly sensitive to \mathbb{Z}_2 symmetry-breaking perturbations [31]. This sensitivity manifests itself through an exponential scaling in size of the steady-state susceptibility, or Green's function. In turn, the particularity of the system causes the signal and noise due to such perturbations to scale differently, leading to an exponentially-large signal-to-noise ratio [31]. Some of these phenomena have recently been observed in optomechanical networks [48] and analog quantum simulation [49].

Remarkably, the exponential scaling of the susceptibility is a NH topological phenomenon. Indeed, the behavior of the susceptibility for one-dimensional driven-dissipative Hamiltonians under open boundary conditions (OBC) is associated with a topological invariant of the dynamical matrix under periodic boundary conditions (PBC) [50]. This leads to so-called topological amplification [51, 52]. Using the singular value decomposition, topological amplification provides a bulk-boundary correspondence [51–53] where the value of the topological invariant corresponds to the number of channels for exponential amplification in the steady state [52]. Such a NH invariant thus appears differently in long-time dynamics than eigenstate-based invariants [54–59].

As with Hermitian systems, the topological phase in NH systems is preserved when the dissipation does not exceed the size of the relevant gap [60], here defined as the

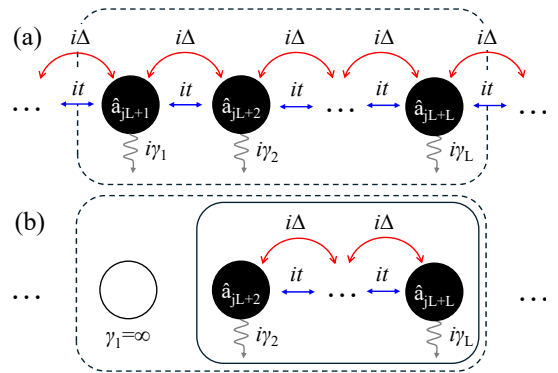


FIG. 1: (a) Schematic of a unit cell (dashed box) of length L for the BKC subject to on-site dissipation $\gamma_j \geq 0$. (b) When $\gamma_1 \rightarrow \infty$, the unit cell effectively becomes an open BKC with $L - 1$ sites (solid box).

minimum distance from the PBC complex energy curve to the origin of the complex energy plane [52]. We find that this criterion, while sufficient, is not a necessary one. While previous studies on the impact of loss in this context focused on uniform dissipation [50, 51, 61, 62], we find cases in which non-uniform dissipation can greatly exceed the above limit. We note that, utilizing these realizations of the BKC as quantum sensors would require the precise delineation of the role of non-uniform loss and this paper takes a step in this direction.

In this work, we study the limits of topological amplification in the bosonic Kitaev chain subject to non-uniform loss. We do this by dividing the system into unit cells of L sites, see Fig. 1 (a).

In Section II, we present the model in more detail and describe topological amplification using the singular value decomposition. We start by applying this framework to the case of uniform dissipation in Section III. We then look at how dissipation affects the PBC spectral curve of the dynamical matrix for different unit cell sizes in Section IV. In Section V, we show that the conventional expectation on robustness to loss can be drastically exceeded: the bosonic Kitaev chain with an even number of sites always exhibits topological amplification provided that loss is placed on every other site. To understand why, we treat this situation in Section V A as a disordered version of the dissipative bosonic Kitaev chain whose unit cell has two sites and where only one is lossy. We find that dissipation induces a topological phase transition only when both sites of the unit cell are allowed to be lossy. Moreover, we show that the PBC energy band splits in two when the absolute difference of the two sites' bath coupling constant exceeds a critical value, but that topological amplification remains as long as one band winds around the origin. Lastly, we study robustness to dissipation in larger unit cells in Section V B.

II. THE BKC MODEL, INPUT-OUTPUT THEORY AND TOPOLOGICAL CLASSIFICATION

The bosonic Kitaev chain [2] is defined as

$$\hat{\mathcal{H}} = \sum_j \left(it\hat{a}_{j+1}^\dagger\hat{a}_j + i\Delta\hat{a}_{j+1}^\dagger\hat{a}_j^\dagger + h.c. \right) \quad (1)$$

where $\hat{a}_j^\dagger, \hat{a}_j$ are the bosonic creation and annihilation operators on site j , respectively, satisfying $[\hat{a}_i, \hat{a}_j^\dagger] = \delta_{i,j}$. We study the model for both periodic boundary conditions (PBC) and open boundary conditions (OBC). The nearest-neighbor hopping t and squeezing Δ are assumed to satisfy $0 < \Delta < t$ as this corresponds to the dynamically stable regime of the open-boundary system [2]. The remarkable features of the model are best understood by considering the \hat{x} and \hat{p} quadratures of the bosonic operators $\hat{a}_j, \hat{a}_j^\dagger$. They are Hermitian operators defined by $\hat{x}_j = (\hat{a}_j + \hat{a}_j^\dagger)/2$ and $\hat{p}_j = (\hat{a}_j - \hat{a}_j^\dagger)/2i$ that obey

$[\hat{x}_i, \hat{p}_j] = i\delta_{i,j}$. In this basis, Eq. (1) becomes

$$\hat{\mathcal{H}} = \sum_j \left((t + \Delta)\hat{x}_j\hat{p}_{j+1} - (t - \Delta)\hat{x}_{j+1}\hat{p}_j \right). \quad (2)$$

As we are interested in studying dynamics, our analysis is centered on the Heisenberg equations of motion

$$\dot{\hat{x}}_j = (t + \Delta)\hat{x}_{j-1} - (t - \Delta)\hat{x}_{j+1}, \quad (3)$$

$$\dot{\hat{p}}_j = (t - \Delta)\hat{p}_{j-1} - (t + \Delta)\hat{p}_{j+1}. \quad (4)$$

A crucial feature of the system is that the quadrature dynamics are completely decoupled and directional: the \hat{x} chain favors movement to the right and the \hat{p} chain favors movement to the left, without ever mixing.

As we want the BKC to act as a quantum amplifier, it is necessary to study how it behaves when it is subject to losses. In the ideal scenario, only the input and output ports are necessary. However, in reality, each site may be lossy. We treat the loss on each site j as due to Markovian baths through coupling constants $\gamma_j \geq 0$. The latter thus correspond to loss rates. Using input-output theory [63], we obtain the Heisenberg-Langevin equations

$$\begin{aligned} \dot{\hat{x}}_j &= (t + \Delta)\hat{x}_{j-1} - (t - \Delta)\hat{x}_{j+1} - \frac{\gamma_j}{2}\hat{x}_j - \sqrt{\gamma_j}\hat{x}_j^{(\text{in})} \\ &\equiv -i \sum_{\ell=1}^N (M_x)_{j,\ell} \hat{x}_\ell - \sqrt{\gamma_j}\hat{x}_j^{(\text{in})} \end{aligned} \quad (5)$$

and

$$\begin{aligned} \dot{\hat{p}}_j &= (t - \Delta)\hat{p}_{j-1} - (t + \Delta)\hat{p}_{j+1} - \frac{\gamma_j}{2}\hat{p}_j - \sqrt{\gamma_j}\hat{p}_j^{(\text{in})} \\ &\equiv -i \sum_{\ell=1}^N (M_p)_{j,\ell} \hat{p}_\ell - \sqrt{\gamma_j}\hat{p}_j^{(\text{in})}, \end{aligned} \quad (6)$$

where $\hat{x}_j^{(\text{in})}$ and $\hat{p}_j^{(\text{in})}$ are the quadratures of the bath input fields on site j and are the operator equivalent of Gaussian white noise. We note that while there is one physical chain, introducing losses does not couple the \hat{x} and \hat{p} dynamics and we can think of \hat{x}_j and \hat{p}_j as two separate non-Hermitian lattices. In the quadrature basis, the full dynamical matrix M is hence block diagonal:

$$M = \begin{pmatrix} M_x & 0 \\ 0 & M_p \end{pmatrix}, \quad (7)$$

with M_x and M_p defined above in Eqs. (5,6). The frequency space quadrature-quadrature susceptibilities in the open-boundary system are defined by

$$\chi^{xx}[\omega] \equiv -i(\omega\mathbf{1} - M_{x,\text{obc}})^{-1}, \quad (8)$$

$$\chi^{xx}[\omega] \equiv -i(\omega\mathbf{1} - M_{p,\text{obc}})^{-1}. \quad (9)$$

Taking the Fourier transform in time of the Heisenberg-Langevin Eqs. (5) and (6) and using the input-output

relations $\hat{x}_j^{(\text{out})} = \hat{x}_j^{(\text{in})} + \sqrt{\gamma_j} \hat{x}_j$ and $\hat{p}_j^{(\text{out})} = \hat{p}_j^{(\text{in})} + \sqrt{\gamma_j} \hat{p}_j$, we find

$$\langle \hat{x}_j^{(\text{out})}[\omega] \rangle = \langle \hat{x}_j^{(\text{in})}[\omega] \rangle + \sum_{\ell=1}^N \sqrt{\gamma_j \gamma_\ell} \chi^{xx}[j, \ell; \omega] \langle \hat{x}_\ell^{(\text{in})}[\omega] \rangle \quad (10)$$

$$\langle \hat{p}_j^{(\text{out})}[\omega] \rangle = \langle \hat{p}_j^{(\text{in})}[\omega] \rangle + \sum_{\ell=1}^N \sqrt{\gamma_j \gamma_\ell} \chi^{pp}[j, \ell; \omega] \langle \hat{p}_\ell^{(\text{in})}[\omega] \rangle \quad (11)$$

where the expectation values are taken with respect to a state obeying the Hamiltonian dynamics. The quadrature susceptibilities relate the quadratures of the output fields to those of the input fields and are hence the relevant quantities to study in order to assess the BKC's ability to act as a quantum amplifier.

We look at how light sent into the system via the first site is amplified as it propagates towards the last site N . To this end, we assume the input to be coherent light with amplitude β whose frequency matches that of the system. Taking its phase to be zero thus amounts to sending light in phase with the \hat{x} quadratures. This is the same setting as in Ref. [31]. We study how the responses on site j , given by $\chi^{xx}[j, 1; \omega]$ and $\chi^{pp}[j, 1; \omega]$, scale with j in the long time limit (or steady state) $\omega = 0$. We note that for the diagonal matrix T with $T_{j,j} = (-1)^j$, the dynamical matrix blocks M_x and M_p satisfy

$$M_{p,\text{obc}} = T M_{x,\text{obc}}^T T. \quad (12)$$

The quadrature susceptibilities then obey

$$\chi^{pp}[j, \ell; \omega] = (-1)^{j+\ell} \chi^{xx}[\ell, j; \omega]. \quad (13)$$

In other words, as long as no perturbation mixes the \hat{x} and \hat{p} dynamics, the amplification properties of the \hat{x} chain will be the same as that of the \hat{p} chain but in the opposite direction. It thus suffices to look at χ^{xx} . What's more, we assume that the coherent signal amplitude β incident upon the chain is much larger than the photon number coming from the baths. For our purposes, this is equivalent to having a zero temperature environment, such that no bath photons come into the system. In this setting, the steady-state average photon number on site j satisfies $\bar{n}_j \equiv \langle a_j^\dagger a_j \rangle_{\text{ss}} \simeq \gamma_1 \beta^2 |\chi^{xx}[j, 1; 0]|^2$, where quantum fluctuations due to amplification are neglected. The response χ^{xx} is then directly linked to the average photon number. As argued in Ref. [31, 34], the quality of an amplifier is intrinsic to its design and must be independent of the total photon number $\bar{n}_{\text{tot}} = \sum_{j=1}^N \bar{n}_j$ in the system. Accordingly, it is sufficient to study the spatial distribution of the average photon number; the BKC will be a good quantum amplifier if $\bar{n}_N / \bar{n}_{\text{tot}} \sim 1$, that is, if photons sent through the first site tend to pile up on the last site in the steady state.

Since the dynamical matrices $M_{x/p}$ are non-Hermitian, complex conjugation and transposition are no longer

equivalent, and the Atland-Zirnbauer classification [64] is no longer applicable to extract their topological invariant. Instead, we consider the classification of NH Hamiltonians given in Ref. [65] and find that the BKC with arbitrary on-site dissipation belongs to the class DIII[†] which has a \mathbb{Z}_2 topological invariant [66]. This invariant corresponds to the winding number ν of the PBC spectral curve $E_{x/p}(k)$ of the dynamical matrix block $M_{x/p}$ about a base point $E_b \in \mathbb{C}$:

$$\nu_{E_b}(E_{x/p}) \equiv \frac{1}{2\pi i} \int_{-\pi}^{\pi} dk \frac{E'_{x/p}(k)}{E_{x/p}(k) - E_b}, \quad (14)$$

since non-Hermiticity allows for the spectrum to be complex. Therefore, certain one-dimensional Hamiltonians can have an energy band that forms a closed loop with nontrivial interior in the complex plane. Such NH Hamiltonians are said to be point-gapped and are known to give rise to a macroscopic number of edge modes in the OBC system [67–71]. The latter phenomenon is called the non-Hermitian skin effect [25, 26]. When the winding number of the PBC curve about the origin $\nu(E_{x/p}) \equiv \nu_{E_b=0}(E_{x/p})$ is nonzero, the OBC edge modes conspire to lead to an amplification (as measured by the susceptibility) that is exponentially large in system size and whose direction is given by the sign of $\nu(E_{x/p})$ [50]. Looking at Eq. (13) we then expect $\nu(E_x) = -\nu(E_p)$. This is confirmed by the fact that Eq. (12) holds under PBC when the total length of the chain N is even. The two PBC spectral curves E_x and E_p are then degenerate and wind in opposite directions. Henceforth, we thus solely concern ourselves with the \hat{x} chain. In passing, we note that the dynamical matrix blocks M_x and M_p are unitarily-equivalent to Hatano-Nelson chains [72, 73] with on-site dissipation.

The connection between the winding number of the PBC spectral curve about the origin and the amplification properties of the system under OBC has been identified as a non-Hermitian bulk-boundary correspondence [52] using the singular value decomposition (SVD) framework outlined in Refs. [51, 53]. The SVD of the dynamical matrix M_x is defined as

$$M_x = U \Sigma V^\dagger = \sum_j \sigma_j |u_j\rangle \langle v_j|, \quad (15)$$

where Σ is a diagonal matrix and the singular values $\sigma_j = \Sigma_{jj}$ are non-negative and uniquely determined by M_x , while U and V are unitary matrices whose columns correspond, respectively, to the left and right singular vectors of M_x . The bulk-boundary correspondence is then stated as follows [52]: a nonzero ν corresponds to $|\nu|$ zero singular values, *i.e.*, singular values σ_j of the OBC system that are exponentially small in system size, and whose associated left and right singular vectors are localized (in system size) at opposite edges. These zero singular modes (ZSMs) thus lead to $|\nu|$ channels for directional amplification, as can most transparently be seen

from the (formal) steady-state response

$$\chi^{xx}[\omega = 0] = iM_x^{-1} = \sum_j \frac{i}{\sigma_j} |u_j\rangle \langle v_j|. \quad (16)$$

The steady-state response $\chi^{xx}[j, 1; 0]$ (and hence the steady-state average photon number \bar{n}_j) on site j induced by driving the first site then scales exponentially with j , provided the amplification channel connects sites 1 and j . Such exponential scaling in the susceptibility is dubbed topological amplification [51]. Naturally, one anticipates this amplification to be robust to some amount of dissipation. We can draw an analogy to disorder in Hermitian systems. In disordered Hermitian systems, we expect that the system stays topological as long as the maximal disorder potential is less than the gap size. In the context of lossy, non-Hermitian systems, it was found that the system remains in its topological phase as long as the maximum on-site loss is smaller than the NH gap of the clean system [60], where the NH gap is defined as the minimum distance from the PBC energies to the origin of the complex plane [52]. In the BKC, we find that in some cases the system can display robustness to loss far beyond this condition.

In this work we study the topological amplification of the BKC subject to dissipation. In particular, we allow for non-uniform, on-site dissipation constants γ_j on each site j which appear on the diagonal of the dynamical matrices M_x and M_p . While the general loss configuration can be studied numerically we progress by reducing the translation invariance of the lattice by introducing repeated unit cells of length L . In this way, the BKC of length N is made up of N/L unit cells whose dissipation constants in Eqs. (5,6) are $\gamma_1, \gamma_2, \dots, \gamma_L \geq 0$. In the dynamical matrix M_x , the dissipation terms are found on the diagonal and satisfy

$$(M_x)_{nL+\ell} = \frac{-i\gamma_\ell}{2}, \quad \ell = 1, 2, \dots, L \quad (17)$$

for all $n = 0, 1, \dots, N/L - 1$. See Fig. 1 (a) for a schematic representation. Our numerical and analytical results show that, for certain bath coupling configurations, the conventional expectation on the robustness of topological phases to disorder outlined in the preceding paragraph is by far exceeded.

III. UNIFORM DISSIPATION, $L = 1$

We first study the topological amplification outlined in the previous section in the BKC whose sites are all subject to the same loss, *i.e.*, $\gamma_j = \gamma \geq 0$ for all j . While such a situation has been touched upon from a topological standpoint in [2, 48–50], the next sections will generalize the treatment to other dissipative configurations. We thus provide details in the case of uniform dissipation for completeness.

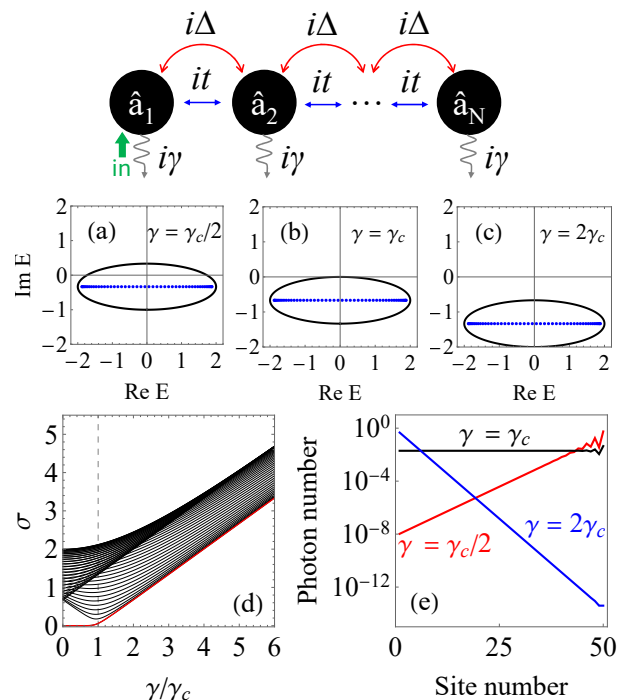


FIG. 2: (a)–(c) Spectrum, (d) singular values and (e) normalized steady-state photon number distribution for the BKC with 50 sites subject to uniform dissipation and input coherent light on the first site. In (a)–(c), the PBC (black) and OBC (blue) spectra of the dynamical matrix M_x are shown for various values of γ . (d) Singular values of the OBC dynamical matrix M_x for 50 sites. The dashed line corresponds to the critical point $\gamma = \gamma_c$. The smallest singular value is highlighted in red and is responsible for the channel of topological amplification as long as $\gamma < \gamma_c$, after which it merges with the rest of the singular spectrum. In all plots $t = 1$ and $\Delta = 1/3$.

The Hamiltonian $\hat{\mathcal{H}}$ with PBC is translation-invariant and we can therefore write it in momentum space:

$$\hat{\mathcal{H}} = \frac{1}{2} \sum_k (\hat{a}_k^\dagger \hat{a}_{-k}) h(k) \begin{pmatrix} \hat{a}_k \\ \hat{a}_{-k}^\dagger \end{pmatrix}, \quad (18)$$

where $h(k)$ is the Bloch Hamiltonian and the dynamical matrix $M(k) = \sigma_z h(k) - i\gamma/2$ is

$$M(k) = (2t \sin(k) - i\gamma/2) \mathbb{1} + 2i\Delta \cos(k) \sigma_x \quad (19)$$

with eigenvalues corresponding to the dynamical matrix blocks $M_{x/p}(k) = 2t \sin(k) + i(\pm 2\Delta \cos(k) - \frac{\gamma}{2})$. In this case, increasing γ shifts the energies down the imaginary axis while leaving the eigenstates invariant. The PBC spectrum of the dynamical matrix encloses the origin of the complex plane as long as $\gamma < \gamma_c \equiv 4\Delta$. As k spans the Brillouin zone, M_x winds clockwise around the origin, while M_p winds counterclockwise, that is, $\nu(M_{x/p}) = \mp 1$. Each non-trivial winding corresponds to a zero singular value of the OBC system. In turn, they lead to two channels that have opposite directional amplification: one for

the \hat{x} chain and the other for the \hat{p} chain. In this setting, a coherent signal sent through the first site results in the steady-state average photon number $\bar{n}_j = \langle \hat{a}_j^\dagger \hat{a}_j \rangle$ being exponentially localized on the last site N of the chain. When the dissipation constant is exactly tuned to the critical value $\gamma/2 = 2\Delta$, the PBC spectrum M_x no longer encloses the origin but touches it at $k = 0$. This is a topological phase transition which can be seen as a closing of the NH gap. In this case, the average photon number distribution is uniform in space. Increasing γ further, the eigenvalues of the dynamical matrix no longer enclose nor touch the origin. The BKC then stops acting as an amplifier and the average photon number distribution localizes on the first site. The three regimes are shown in Fig. 2 and explicit calculations of the average photon distribution in the steady state are given in Appendix A. The critical value can be found by looking for a zero energy state of the PBC spectrum of M_x or by looking for a zero singular value of M_x which is the gap closure of a Hermitian system described by $M_x^\dagger M_x$. We show this in the next section.

IV. PH SYMMETRY AND PBC SPECTRAL BANDS

We now turn our attention to systems with reduced translation symmetry. The chain is divided into unit cells of size L and the bath coupling constants γ_j may vary within the unit cell. This can lead to the system having more than one PBC energy band. However, regardless of the values of γ_j , the spectrum of the dynamical matrix block M_x under both OBC and PBC is symmetric about the imaginary axis. That is, M_x obeys the non-Hermitian particle-hole symmetry known as PHS[†] [65]

$$M_x = -M_x^* \quad (20)$$

which follows readily from the fact that M_x has strictly imaginary entries [74]. When there is no dissipation, the spectrum of M_x under OBC is real—which is ensured by the stability assumption, $0 < \Delta < t$ [2]. The particle-hole symmetry of Eq. (20) hence guarantees a zero-energy mode in the clean system when its total length is odd. We keep this in mind when analyzing the dissipative chain.

We now turn our attention to the dissipation in a system made up of L/N unit cells of length L where the dissipation is only on the first site in each unit cell meaning that $\gamma_1 > 0$ and $\gamma_j = 0$ for $L \geq j \geq 2$.

On the one hand, when $\gamma_1 = 0$, there is no dissipation and the spectral curve of $M_{x,\text{pbc}}$ winds around the origin. On the other hand, in the asymptotic limit $\gamma_1 \rightarrow \infty$, the PBC and OBC systems effectively break into N/L copies of a dissipationless BKC with $L-1$ sites and open boundary conditions. One can view this as disconnecting the first site of each unit cell, on which there will be a localized mode of energy $-i\gamma_1/2$. Indeed, as soon as a particle hops on the first site, it directly leaks into the environment, such that neighboring unit cells no longer commu-

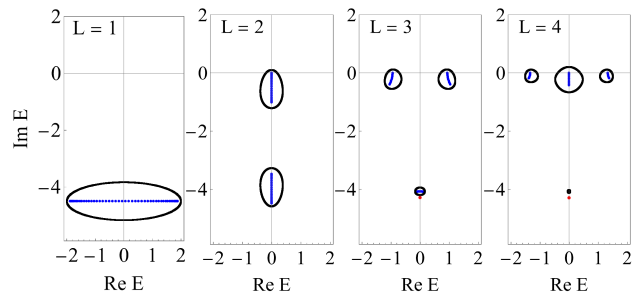


FIG. 3: Spectrum of the dynamical matrix M_x for OBC (blue) and PBC (black) for different unit cell lengths L whose first site is subject to loss. When γ_1 is large enough, the PBC curve splits into L bands. For $L = 3, 4$, the red point corresponds to the OBC eigenenergy that lies outside of the PBC spectral curve. In all plots $t = 1$, $\Delta = 1/3$ and $\gamma_1 = 9$.

nicate, see Fig. 1 (b). Since there is no dissipation on the remaining sites, the spectrum of the dynamical matrix block $M_{x,\text{obc}}$ associated with the BKC of length $L-1$ is real. When $L-1$ is odd, the PHS[†] of Eq. (20) ensures the existence of a zero energy mode. Therefore, as γ_1 is increased from zero, N/L eigenenergies of M_x tend to the origin of the complex plane. Since the spectrum of $M_{x,\text{pbc}}$ winds around the origin at $\gamma_1 = 0$, we anticipate the PBC spectral curve to keep winding around the origin as γ_1 is increased when L is even, but not when L is odd. Additionally, N/L energies tend to $-i\infty$ as $\gamma_1 \rightarrow \infty$. Using Gershgorin's circle theorem [75] on $M_{x,\text{pbc}}$, we find that the PBC spectral curve corresponds to at least two bands when $\gamma_1 > 8t$. In fact, we numerically observe that the PBC spectral curve of the BKC with unit cell length L splits into L bands when γ_1 is large enough, see Fig. 3.

No matter the number of bands or whether the PBC spectral curve winds around the origin, we numerically observe the NH skin effect when $\gamma_1 \geq 0$ is small enough. That is, the spectrum of $M_{x,\text{obc}}$ lies inside the PBC spectral curve and all of the OBC eigenstates are localized on the last site of the chain. However, for $L > 2$, as γ_1 is increased past a critical value $\zeta > 0$, there is a single OBC eigenenergy that leaves the area enclosed by the PBC spectral curve, see the red points in Fig. 3. In more rigorous terms, the winding number of the PBC spectral curve about this OBC eigenenergy changes when $\gamma_1 = \zeta$. Furthermore, the associated OBC eigenstate transitions from a NH skin mode localized on the last site N when $\gamma_1 < \zeta$ to a completely delocalized state at $\gamma_1 = \zeta$ and to an edge state localized on the other boundary $j = 1$ when $\gamma_1 > \zeta$. The details of this OBC mode are provided in Appendix B. We note that the behavior of this mode is not tied to the topological phases of amplification.

V. TOPOLOGICAL AMPLIFICATION, TOPOLOGICAL INVARIANTS AND THE BKC WITH REDUCED PERIODICITY

As a hallmark of non-trivial topological phases, the channels of exponential amplification are generally robust to disorder for driven-dissipative systems. This is guaranteed provided that the size of the non-Hermitian gap is larger than the maximum amount of disorder present in the system [60]. While this is a sufficient condition, we show that in certain cases, the BKC exhibits exponential amplification even if the maximum disorder value exceeds the NH gap. We find that when the total length of the chain N is even, the nontrivial topological phase responsible for exponential amplification remains for arbitrarily large loss on odd sites γ_{2j+1} , see Fig. 4. Moreover, we show that the intuition outlined in the previous section is borne out: when L is odd, dissipation on the first site of the unit cells is enough to induce a topological phase transition, while this is not true when L is even. This is demonstrated by observing the NH spectrum of the system with $\gamma_1 \geq 0$ as seen in Fig. 5 and Fig. 6 for $L = 2$, and Fig. 7 for $L = 3$. Without dissipation the spectrum winds around the origin. Then upon increasing γ_1 the spectrum splits into L disconnected curves. These curves become smaller as γ_1 is increased and winds around their $\gamma_1 \rightarrow \infty$ value. This means one curve winds around $-i\gamma/2$ and $L - 1$ curves wind around the (real) solutions of a non-dissipative BKC with $L - 1$ sites and open boundary conditions. It is therefore expected that when $L - 1$ is odd (even unit cell length) one of the disconnected curves will always wind around the origin as the clean $L - 1$ chain with OBC has a zero energy solution.

A. Unit Cell With $L = 2$ Sites

To explain the surprising robustness to disorder depicted in Fig. 4, we first consider the case where the unit cell of the BKC has two sites. In momentum space, the block matrix $M_x(k)$ is

$$M_x(k) = \begin{pmatrix} -\frac{i\gamma_1}{2} & i(t + \Delta)e^{-ik} - i(t - \Delta) \\ i(t + \Delta) - i(t - \Delta)e^{ik} & -\frac{i\gamma_2}{2} \end{pmatrix},$$

where $k \in (-\pi, \pi)$ is confined to the reduced Brillouin zone and we set the lattice constant $2a = 1$. Of course, taking $\gamma_1 = \gamma_2$ reduces to the case of uniform dissipation. The eigenvalues are found to be

$$E_{\pm}(k) = -\frac{i\gamma_{\pm}}{4} \pm i\sqrt{\frac{\gamma_{\pm}^2}{16} - 2(t^2 - \Delta^2) + (t + \Delta)^2e^{-ik} + (t - \Delta)^2e^{ik}}. \quad (21)$$

where $\gamma_{\pm} \equiv \gamma_1 \pm \gamma_2$ and the principal square root is understood. Importantly, the curves E_+ and E_- do not

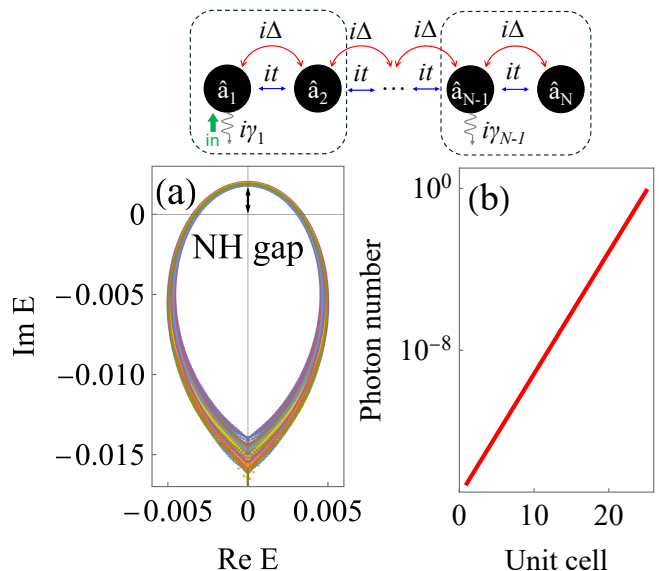


FIG. 4: (a) The (complex) spectrum of the dynamical matrix under PBC for the BKC with 1000 sites (500 unit cells) whose odd sites exhibit loss sampled from the uniform distribution $\gamma_{2j+1}/t \in [0, 1000]$. Each color of points represents one of the 100 runs with a different realization of disorder. The system is always in a nontrivial topological phase; the NH gap remains open for all 100 runs with the origin inside the energy band. (b) Normalized steady-state photon number distribution $\langle \hat{a}_j^\dagger \hat{a}_j \rangle \propto |\chi^{xx}[j, 1; \omega = 0]|^2$ for the BKC under open boundary conditions (OBC) with 50 sites (25 unit cells). The photon distribution is exponentially localized on the last unit cell and is independent of $\gamma_1, \gamma_3, \dots, \gamma_{N-1}$.

constitute parts of a single closed curve for all parameter values. We already know that they form a closed loop when $\gamma_1 = \gamma_2$, see Fig. 2. However, the situation becomes very different when $\gamma_- \neq 0$. Analysis of the spectrum in Eq. 21 shows that the solutions split into two curves when $|\gamma_-| > 8t$ as can be seen in Fig 5. In this region the spectrum develops a line gap. We remark that when $\gamma_2 = 0$, the critical value $\gamma_- = \gamma_1 = 8t$ is exactly that identified using the Gershgorin circle theorem [75] estimate in Section IV. Since a line gap is defined as a line in the complex-energy plane that does not cross the spectrum and has energy values on either side, the critical value $|\gamma_-| = 8t$ separates a regime where there is no line gap in the PBC system from one where there is. However, in our setting, the emergence of such a line gap is not topological. Indeed, even when the energy levels E_{\pm} do not form closed curves on their own, we can still compute their contribution to the winding number $\nu(E_{\pm})$ using Eq. (14), which obey $\nu(E) = \nu(E_+) + \nu(E_-)$. Using the argument principle, the winding number $\nu(E)$ satisfies $\nu(E) = Z - P$, where Z and P are the number

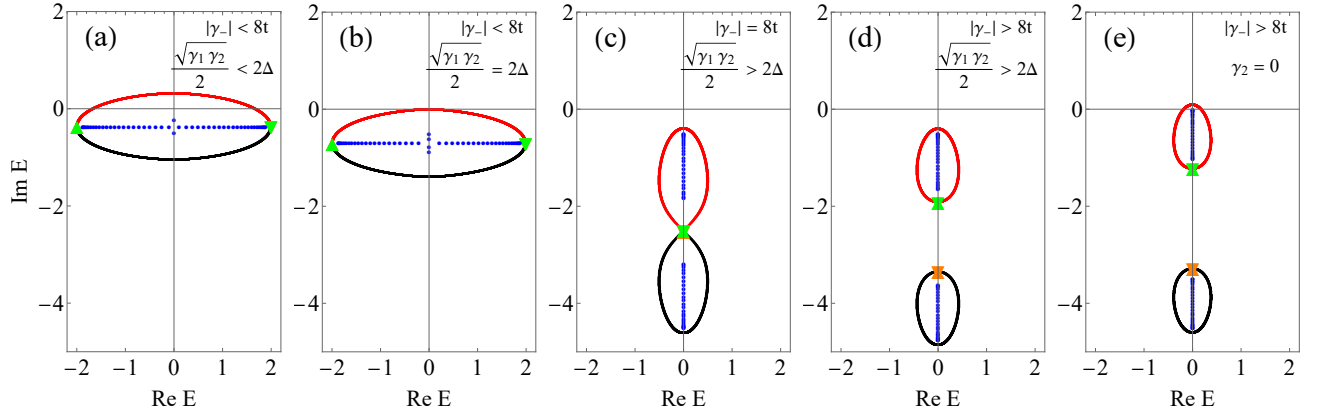


FIG. 5: Spectra of the dynamical matrix block M_x for the two-site unit cell BKC for various values of bath coupling constants $\gamma_1 \geq 0$ and $\gamma_2 \geq 0$. The OBC spectrum (blue) is for a chain of 50 sites. The red (black) curve corresponds to the part of the PBC spectrum given by E_+ (E_-), see Eq. (21). The PBC spectrum is subject to two independent processes: it winds around the origin depending on how $\frac{\sqrt{\gamma_1 \gamma_2}}{2}$ relates to 2Δ , while the presence of a line gap is associated with how $|\gamma_-| \equiv |\gamma_1 - \gamma_2|$ compares to $8t$. Further, \blacktriangle corresponds to $\lim_{k \downarrow -\pi} E_+(k)$ and \blacktriangledown corresponds to $\lim_{k \uparrow \pi} E_+(k)$. When visible, \blacktriangle overlaps with \blacktriangle and \blacktriangledown overlaps with \blacktriangledown . See Section V A for details. Panels (a)–(d) have $\gamma_2 = 1$ while (e) has $\gamma_2 = 0$. (a) $\gamma_1/2 = 2\Delta^2$. (b) $\gamma_1/2 = 4\Delta^2$. (c) $\gamma_1 = 9$. (d) $\gamma_1 = 9.5$. (e) $\gamma_1 = 9$. In all plots $t = 1$ and $\Delta = 1/3$.

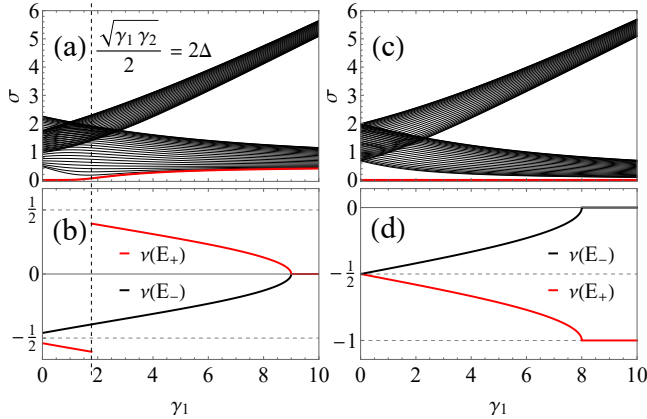


FIG. 6: Singular values [(a) and (c)] and winding number contributions [(b) and (d)] of the two-site unit cell BKC dynamical matrix block M_x as a function of the bath coupling constant γ_1 , see Fig. 5 for the spectra. The singular values σ are those of the 50-site open BKC, with the smallest singular value in red. (a)–(b) The unit cell's second site has $\gamma_2 = 1$ allowing for a topological phase transition at $\frac{\sqrt{\gamma_1 \gamma_2}}{2} = 2\Delta$, depicted by the vertical dashed line. The emergence of a line gap in the PBC system happens at $\gamma_1 = 9$, at which point the absolute difference in losses satisfies $|\gamma_-| = 8t$. (c)–(d) The unit cell's second site shows no loss $\gamma_2 = 0$. In this case, the system exhibits no topological phase transition; the winding number $\nu(E) = \nu(E_+) + \nu(E_-) = -1$ for all $\gamma_1 \geq 0$ and the emergence of a line gap happens at $\gamma_1 = 8$. See Section V A for more details. In all plots $t = 1$ and $\Delta = 1/3$.

of zeroes and poles of

$$E(z) = -\frac{i\gamma_+}{4} \pm \frac{i}{4} \sqrt{\gamma_-^2 - 32(t^2 - \Delta^2) + \frac{16(t + \Delta)^2}{z} + 16(t - \Delta)^2 z}$$

within the unit circle, respectively. There is evidently a pole at $z = 0$. For the zeroes, we find

$$z_{\pm} = \frac{\gamma_1 \gamma_2 + 8(t^2 - \Delta^2) \pm \sqrt{\gamma_1^2 \gamma_2^2 + 16\gamma_1 \gamma_2 (t^2 - \Delta^2)}}{8(t - \Delta)^2}.$$

Although we always have $|z_+| > 1$ as long as $0 < \Delta < t$ and $\gamma_1 \gamma_2 > 0$, the zero z_- lies inside the unit circle when $\frac{\sqrt{\gamma_1 \gamma_2}}{2} > 2\Delta$, and outside when $\frac{\sqrt{\gamma_1 \gamma_2}}{2} < 2\Delta$. Thus

$$\nu(E) = \begin{cases} -1 & \frac{\sqrt{\gamma_1 \gamma_2}}{2} < 2\Delta, \\ 0 & \frac{\sqrt{\gamma_1 \gamma_2}}{2} > 2\Delta. \end{cases} \quad (22)$$

The value $\frac{\sqrt{\gamma_1 \gamma_2}}{2} = 2\Delta$ is hence identified as the point at which the NH gap closes and can also be found by requiring a zero mode in the PBC spectral curve or singular spectrum. When $\gamma_2 = 0$ ($\gamma_1 = 0$), the PBC spectral curve always winds around the origin and $\nu(E) = -1$ for all $\gamma_1 \geq 0$ ($\gamma_2 \geq 0$), as shown in Fig. 5 (e). We conclude that there are two processes at play simultaneously: the emergence of a line gap at $|\gamma_-| = 8t$, see Fig. 5 (c)–(d), and the topological phase transition at $\frac{\sqrt{\gamma_1 \gamma_2}}{2} = 2\Delta$, see Fig. 5 (b). Interestingly, these two processes are independent of each other since one depends exclusively on t and the other on Δ . As long as there is a

PBC energy band winding around the origin, the system exhibits topological amplification regardless of whether there exists a line gap. We note that this is a consequence of our setting and may not always be true; in Appendix D, we show that the line gap can be topological if we add gain on every site. When $\frac{\sqrt{\gamma_1\gamma_2}}{2} < 2\Delta$, the BKC with a two-site unit cell hosts two zero singular modes, one associated with the \hat{x} chain and the other with the \hat{p} chain, see Fig. 6. In turn, these ZSMs lead to two channels for exponential amplification whose directions are opposite. This means that any γ_1 , as large as it may be, can be compensated by reducing γ_2 to remain in the topological phase of exponential amplification. For completeness, we analytically verify that there is exponential amplification when $\frac{\sqrt{\gamma_1\gamma_2}}{2} < 2\Delta$ using the system's susceptibility in Appendix C. At the critical value $\frac{\sqrt{\gamma_1\gamma_2}}{2} = 2\Delta$, the \hat{x} chain hosts a zero energy eigenstate of $M_{x,\text{pbc}}$ with zero momentum. It is readily found to be $|\psi_0\rangle = \bigotimes_{j=1}^{N/2} |\phi_0\rangle$, where the intra-unit cell vector $|\phi_0\rangle$ is $|\phi_0\rangle = \frac{1}{\mathcal{N}}(\gamma_2/4\Delta, 1)^T$ with normalizing constant $\mathcal{N} = \sqrt{1 + \gamma_2^2/\gamma_1^2}$.

The fact that the system exhibits exponential amplification for all values of γ_1 as long as $\gamma_2 = 0$ far exceeds the expectation that a topological phase transition will occur when the maximum disorder value surpasses the size of the NH gap [60]. The topological amplification is then insensitive to the losses on the chain's odd sites. In fact, we may as well allow for arbitrary bath coupling constants $\gamma_1, \gamma_3, \dots, \gamma_{N-1}$ on the odd sites of the chain. This is the essence behind Fig. 4, where the dissipation on the even sites is zero while the dissipation on the odd sites is random and yet, the spectrum winds around the origin. To understand why this generalization works, consider the spectrum of the periodic dynamical matrix blocks M_x . When the odd bath coupling constants $\gamma_1, \gamma_3, \dots, \gamma_{N-1} \geq 0$ are small enough, the PBC spectrum winds around the origin and the OBC system exhibits exponential amplification. For a topological phase transition to occur for certain values of odd bath coupling constants, the PBC spectral curve must cross the origin and a zero energy mode must exist. That is, there must be some $k \in (-\pi, \pi)$ at which $M_x(k)|\psi_0\rangle = 0$ for some $|\psi_0\rangle = (\psi_1, \dots, \psi_N)$. Explicitly,

$$i(t + \Delta)\psi_{2j} - i(t - \Delta)\psi_{2j+2} - \frac{i\gamma_{2j+1}}{2}\psi_{2j+1} = 0 \quad (23)$$

$$i(t + \Delta)\psi_{2j-1} - i(t - \Delta)\psi_{2j+1} = 0, \quad (24)$$

for $1 \leq j \leq \frac{N-2}{2}$. However, one can prove that such a state cannot exist. Indeed, letting $r > 0$ be defined by $e^{2r} = \frac{t+\Delta}{t-\Delta}$, Eq. (24) yields $\psi_{2j+1} = e^{2r}\psi_{2j-1}$. Since $N-1$ is odd, we find $\psi_{N-1} = e^{r(N-2)}\psi_1$. However, the PBC gives $\psi_1 = e^{2r-ik}\psi_{N-1}$ meaning $\psi_{2j+1} = 0$ for all j . Thus, Eq. (23) yields $\psi_{2j+2} = e^{2r}\psi_{2j}$ and, similarly, we find $\psi_{2j} = 0$. Therefore, the fact that the eigenstates are exponentially localized on the edge under OBC is exactly what prevents the PBC spectrum from containing a

zero energy eigenstate. We conclude that, no matter the values of the odd bath coupling constants, $M_{x,\text{pbc}}$ never has a zero energy eigenstate, and hence that the PBC spectral curve never crosses the origin as $\gamma_1, \gamma_3, \dots, \gamma_{N-1}$ are increased from zero. The system is thus always in a nontrivial topological phase. In other words, no matter the on-site losses that are introduced on the odd sites, the system whose length is even will always exhibit exponential amplification. We prove this statement using the susceptibility via a repeated application of Dyson's equation in Appendix E.

B. Unit Cell With $L > 2$

We now consider the BKC with a unit cell of more than two sites and with dissipation only on its first site. We look at whether there is a specific $\gamma_1 > 0$ at which dissipation will induce a topological phase transition out of the phase of exponential amplification. To this end, we separate the general situation $L > 2$ into two cases: one where L is even and one where L is odd.

1. Even L

When the length of the unit cell is even, the total length of the chain N is always even, regardless of the number of unit cells N/L . Therefore, a chain with even L and nonzero dissipation γ_1 on the first site of its unit cells is a chain with an even length and nonzero dissipation on certain odd sites. From the previous section, we know that, as long as $\gamma_2 = \gamma_4 = \dots = \gamma_N = 0$, no amount of loss on the odd sites of a chain with even length can induce a topological phase transition out of the exponentially-amplifying phase. Therefore, for any even L , there will be topological amplification for any amount of loss $\gamma_1 > 0$. This confirms the intuition provided in Section IV.

2. Odd L

The situation when L is odd is drastically different from when L is even; we find that one lossy site per unit cell is sufficient to induce a topological phase transition, see Fig. 7. When γ_1 is small enough, the system is in a non-trivial topological phase, with the spectrum of the dynamical matrix winding around the origin [Fig. 7 (a)]. In this setting, there is a zero singular mode of $M_{x,\text{obc}}$ whose singular value, depicted in red in Fig. 7 (d), leads to a channel for exponential amplification in the open chain. The average photon distribution is then exponentially localized on the last unit cell. As γ_1 is increased, more and more particles dissipate into the environment preventing them from reaching the end of the chain. At some critical value $\gamma_1 = \gamma_c$, the dissipation is such that for a photon starting on the first site of a given unit cell,

the non-reciprocity is perfectly nullified by the dissipation. In this case, the photons are uniformly distributed between the unit cells [Fig. 7 (e)]—although they might not be uniformly distributed within each unit cell. It is at this point that there is a topological phase transition and that the PBC spectral curve touches the origin. To find the critical value γ_c we look for a zero energy state of the PBC chain. Since the system is periodic with a unit cell of L sites this reduces to finding the determinant of an $L \times L$ (dynamical) matrix and equating it to zero. Alternatively, we can solve the following difference equations for the wavefunction $\psi_{n,j}^{(k)} = e^{ikn}\phi_j$ where j represents the position within the unit cell, n is the unit cell number related to the lattice momentum k .

$$i(t + \Delta)\phi_{j-1} - i(t - \Delta)\phi_{j+1} = 0, \quad j \neq 1, L \quad (25)$$

$$i(t + \Delta)e^{-ik}\phi_L - i(t - \Delta)\phi_2 - \frac{i\gamma_c}{2}\phi_1 = 0, \quad (26)$$

$$i(t + \Delta)\phi_{L-1} - i(t - \Delta)e^{ik}\phi_1 = 0. \quad (27)$$

Recalling that $e^{2r} = \frac{t+\Delta}{t-\Delta}$, the three equations above lead to the following equation:

$$(t + \Delta)e^{-ik}e^{r(L-1)} - (t - \Delta)e^{ik}e^{-r(L-1)} = \frac{\gamma_c}{2}. \quad (28)$$

The requirement that γ_c is real leads to $k = \pm\pi$ and since γ_c is positive only the $k = 0$ is possible. This finally leads to the simple condition:

$$\frac{\gamma_c}{2} = (t + \Delta)e^{r(L-1)} - (t - \Delta)e^{-r(L-1)}. \quad (29)$$

Since the critical value γ_c given in Eq. (29) is valid for any odd length unit cell, it must also be valid for a unit cell of one site. Indeed, setting $L = 1$, we retrieve the critical value of the uniform case found in Section III.

VI. CONCLUSION

We have shown that the phase-dependent topological amplification of a coherent signal sent into one end of the open BKC is remarkably robust to on-site losses. It persists for arbitrarily large losses on every other site when the length of the chain is even, drastically exceeding conventional expectations. To understand why, we looked at uniform and non-uniform dissipation where the system is divided into N/L unit cells of length L . Using the complex spectrum of the periodic dynamical matrix as well as the singular values and the susceptibility of the open dynamical matrix, we have found exact dissipation values at which a topological phase transition occurs for various unit cell lengths and bath coupling configurations. When the unit cell has two sites, we show that there is a critical value at which the difference in on-site dissipation induces a PBC energy band separation. Nonetheless, exponential amplification is observed

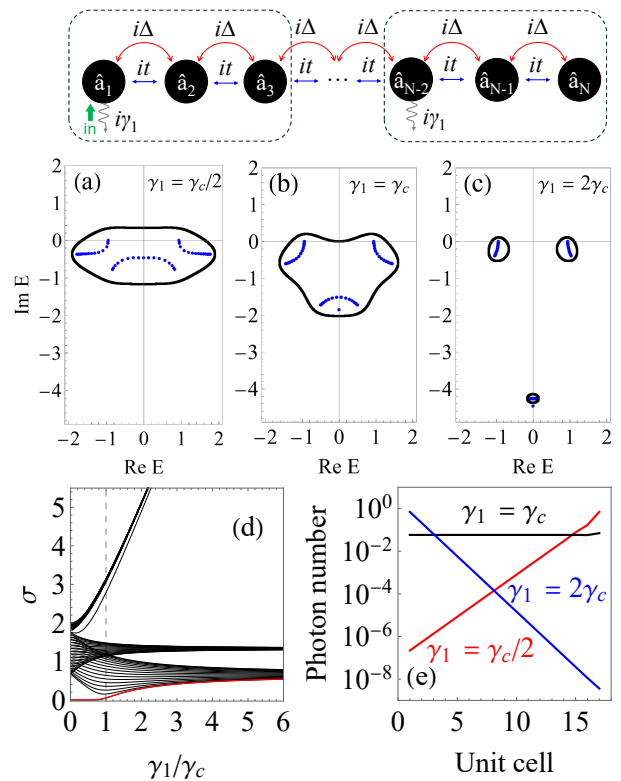


FIG. 7: (a)–(c) Spectrum, (d) singular values and (e) normalized steady-state unit cell photon number distribution for the three-site unit cell BKC with 51 sites (17 unit cells) and loss on every three sites. In (a)–(c), the PBC (black) and OBC (blue) spectrum of M_x are shown for different values of the bath coupling constant γ_1 , showcasing a topological phase transition. (d) The singular values are plotted for the dynamical matrix block M_x of the (open) BKC with 51 sites as a function of the bath coupling constant γ_1 . The critical point $\gamma_1 = \gamma_c$ is depicted by the vertical dashed line and separates a regime wherein the smallest singular value (red) is exponentially small in system size from one in which it is not. See Section VB 2 for details. In all plots $t = 1$ and $\Delta = 1/3$, so that the critical value Eq. (29) yields $\gamma_c = 14/3$.

as long as one PBC band winds around the origin in the complex plane. The system transitions out of the exponentially-amplifying topological phase when the geometric mean of the on-site dissipation of the two sites equals twice the nearest-neighbor drive: $\sqrt{\gamma_1\gamma_2}/2 = 2\Delta$. As such, the non-trivial topological phase of exponential amplification can be guaranteed by compensating an arbitrarily large dissipation on the first site by an arbitrarily small dissipation on the second. Looking at larger unit cells, we then separated our analysis between even and odd $L > 2$. We showed that dissipation on the first site of unit cells of even length is never enough to induce a phase transition out of the exponentially-amplifying phase. In contrast, it is enough for odd length unit cells and we find the critical value at which it happens. We explain this

discrepancy via a non-Hermitian particle-hole symmetry and by looking at the limit of infinite loss on the first sites. All in all, our work demonstrates that the BKC is a promising quantum sensor—one that showcases strong signal amplification while being robust to disorder.

ACKNOWLEDGMENTS

We thank Alexander McDonald and Evgeny Moiseev for useful discussions. The authors are supported by NSERC and FRQNT. We acknowledge the support from Québec's Ministère de l'Économie, de l'Innovation et de l'Énergie (MEIE) and Photonique Quantique Québec (PQ2).

Appendix A: Photon Distribution for Uniform Dissipation

To find an analytical expression of the photon distribution of the BKC subject to uniform dissipation, it is useful to consider the on-site squeezing transformation

$$\hat{U} = \prod_{j=1}^N \exp \left[\frac{r(j-j_0)}{2} (\hat{a}_j \hat{a}_j - \hat{a}_j^\dagger \hat{a}_j^\dagger) \right] \quad (\text{A1})$$

where the squeezing parameter $r > 0$ is defined by the ratio $e^{2r} \equiv \frac{t+\Delta}{t-\Delta}$ and j_0 is an arbitrary real number. Under this unitary transformation the BKC Hamiltonian of Eq. (1) becomes

$$\hat{\mathcal{H}} \equiv \hat{U} \hat{\mathcal{H}} \hat{U}^\dagger = i\tilde{t} \sum_{j=1}^{N-1} (\hat{a}_{j+1}^\dagger \hat{a}_j - \hat{a}_j^\dagger \hat{a}_{j+1}) \quad (\text{A2})$$

where $\hat{a}_j = \cosh(rj)\hat{a}_j + \sinh(rj)\hat{a}_j^\dagger$ are the squeezed bosonic operators and $\tilde{t} \equiv \sqrt{t^2 - \Delta^2} = t/\cosh(r)$ is an imaginary hopping parameter. The dissipationless BKC is thus unitarily-equivalent to a simple particle-conserving tight-binding model. Crucially, the quadrature susceptibilities in Eqs. (8) and (9) are given by

$$\chi^{xx}[j, \ell; \omega] = e^{r(j-\ell)} \tilde{\chi}[j, \ell; \omega], \quad (\text{A3})$$

$$\chi^{pp}[j, \ell; \omega] = e^{-r(j-\ell)} \tilde{\chi}[j, \ell; \omega], \quad (\text{A4})$$

where the frequency space susceptibility $\tilde{\chi}$ of the tight-binding Hamiltonian of Eq. (A2) of is known to be [31]

$$\tilde{\chi}[j, \ell; \omega] = i^{j-\ell+1} \frac{U_{\min(j,\ell)-1}(\frac{\omega}{2\tilde{t}}) U_{N-\max(j,\ell)}(\frac{\omega}{2\tilde{t}})}{\tilde{t} U_N(\frac{\omega}{2\tilde{t}})} \quad (\text{A5})$$

where U_n is the Chebyshev polynomial of the second kind of degree n . Adding uniform dissipation $\gamma \geq 0$ on each site amounts to shifting the frequency $\omega \rightarrow \omega + i\gamma/2$

in $\tilde{\chi}$. The zero frequency (steady-state) response terms necessary to compute the average photon number are

$$\tilde{\chi}[j, 1; 0] = \frac{i^j U_{N-j}(i\frac{\gamma}{4\tilde{t}})}{\tilde{t} U_N(i\frac{\gamma}{4\tilde{t}})}. \quad (\text{A6})$$

The Chebyshev polynomial U_n have the closed form

$$U_n(x) = \frac{(x + \sqrt{x^2 - 1})^{n+1} - (x - \sqrt{x^2 - 1})^{n+1}}{2\sqrt{x^2 - 1}}. \quad (\text{A7})$$

Setting $x = \frac{\gamma}{4\tilde{t}}$ and $y = x + \sqrt{x^2 + 1}$, we find

$$U_n(ix) = \frac{i^n}{2\sqrt{x^2 + 1}} [y^{n+1} - (-y)^{-(n+1)}]. \quad (\text{A8})$$

As $y \geq 1$, the susceptibility terms for $N - j + 1 \gg 1$ can be written as

$$\tilde{\chi}[j, 1; 0] = \frac{y^{N-j+1} - (-y)^{-(N-j+1)}}{\tilde{t}(y^{N+1} - (-y)^{-(N+1)})} \simeq \frac{1}{\tilde{t}y^j}. \quad (\text{A9})$$

Since the average photon number is $\bar{n}_j \propto |\chi^{xx}[j, 1; 0]|^2$, we use Eq. (A3) to find that

$$\bar{n}_j \propto \frac{1}{(t + \Delta)^2} \left(\frac{e^r}{y} \right)^{2j}. \quad (\text{A10})$$

The critical value $y_c = e^r$ is equivalent to $\gamma/2 = 2\Delta$ and corresponds to the case of uniform average photon distribution in the chain. When $y < e^r$, we have $\gamma/2 < 2\Delta$ and the photons localize exponentially on the last site of the chain. Lastly, $y > e^r$ corresponds to the situation of high dissipation $\gamma/2 > 2\Delta$ wherein photons are exponentially localized on the first site.

Appendix B: Localization Transition

Here we provide details on the eigenstate identified in Section IV that undergoes a transition in the edge on which it is localized. As mentioned in the main text, this state is an eigenstate of the open BKC whose unit cells of length $L > 2$ are subject to loss $\gamma_1 > 0$ on their first site. We observe that there is a critical value $\gamma_1 = \zeta > 0$ below which the eigenstate is localized on the edge N with its energy inside the PBC spectral curve and above which it is localized on the other edge $j = 1$ with its energy outside the PBC spectral curve. We emphasize that this eigenstate and its localization transition are not associated with the topological phase of amplification. To illustrate that such a state exists analytically, we focus on the case $L = 3$ with semi-infinite boundary conditions (SIBC). We find ζ and show that the localization transition is equivalent to a change in the winding number of the PBC spectral curve about the energy of the SIBC eigenstate. Denote this eigenstate by $|\psi\rangle = \otimes_j z^j |\phi\rangle$

where $|\phi\rangle = (\phi_1, \phi_2, \phi_3)^T$ is the intra-unit-cell eigenstate and $z = z(\gamma_1)$ satisfies

$$|z(\gamma_1 < \zeta)| > 1, \quad |z(\gamma_1 > \zeta)| < 1 \quad (\text{B1})$$

with $|z(\gamma_1 = \zeta)| = 1$ for some $\zeta > 0$. To obtain an expression for ζ , we solve the intra-unit-cell equation $M_x(z)|\phi\rangle = i\epsilon|\phi\rangle$ by imposing $|z(\gamma_1 = \zeta)| = 1$. Making the (numerically-informed) ansatz $\phi_3 = 0$, we find

$$\frac{\zeta}{2} = \frac{(t + \Delta)^3 + (t - \Delta)^3}{(t + \Delta)(t - \Delta)}. \quad (\text{B2})$$

Comparing with the loss rate at which there is a topological phase transition γ_c given in Eq. (29), we find that $\zeta > \gamma_c$, since $t > \Delta > 0$. In other words, the localization transition always happens after the topological phase transition. To show that there is a z that satisfies Eq. (B1), we solve $M_x(z)|\phi\rangle = i\epsilon|\phi\rangle$ again but for z in terms of γ_1/ζ to find

$$z_{\pm} = \frac{\gamma_1}{\zeta} \left(\frac{\pm \sqrt{(e^{6r} + 1)^2 - 4e^{6r} \frac{\zeta^2}{\gamma_1^2} - (e^{6r} + 1)}}{2} \right) \quad (\text{B3})$$

where $e^{2r} = \frac{t+\Delta}{t-\Delta}$. While $|z_-| > 1$ for all γ_1 , we note that z_+ satisfies $z(\gamma_1 = \zeta) = -1$ as well as Eq. (B1). Moreover, the energy of the mode $|\psi\rangle$ for $\gamma_1 > 0$ is

$$i\epsilon = -\frac{i\gamma_1}{4} \left(1 + \sqrt{1 - \frac{16(t^2 - \Delta^2)}{\gamma_1^2}} \right), \quad (\text{B4})$$

which is $i\epsilon \simeq -\frac{i\gamma_1}{2}$ when $\gamma_1/2 \gg 2\sqrt{t^2 - \Delta^2}$. Finally, the intra-unit-cell eigenstate $|\phi\rangle$ is

$$|\phi\rangle = \frac{1}{\mathcal{N}} (1 \quad \frac{t+\Delta}{\epsilon} \quad 0)^T. \quad (\text{B5})$$

We now show the equivalence between the localization transition of the SIBC eigenstate $|\psi\rangle$ and the change in winding number of the PBC spectral curve about the eigenstate's energy $i\epsilon$. Using Eq. (14), the argument principle gives that the winding number $\nu_{i\epsilon}(E)$ of the PBC curve $E = E(k)$ for $k \in (-\pi, \pi)$ about the point $i\epsilon \in \mathbb{C}$ is $\nu_{i\epsilon}(E) = Z - P$, where Z and P are the zeroes and poles of $\tilde{E}(z) = E(z) - i\epsilon$ within the unit circle, respectively. While the zeroes correspond to when $E(z) = i\epsilon$, the number of poles of $\tilde{E} = \tilde{E}(z)$ corresponds to that of $E = E(z)$ since $i\epsilon$ is independent of z . From the characteristic equation $\det(M_x(z) - E) = 0$, the function $E = E(z)$ possesses the single pole $z = 0$ due to the matrix entry $-i(t - \Delta)z^{-1}$. Further, the number of $z \in \mathbb{C}$ with $|z| < 1$ that satisfy $E(z) = i\epsilon$ can be obtained by solving the characteristic equation $\det(M_x(z) - i\epsilon) = 0$. One then obtains $z = z(\gamma_1)$ given by Eq. (B3). From Eq. (B1), we know that $\gamma_1 = \zeta$ separates a regime where z_+ lies outside of the unit circle to one where it lies inside. Therefore, the value $\gamma_1 = \zeta$ separates two phases

with different winding number:

$$\nu_{i\epsilon}(E) = \begin{cases} -1 & \gamma_1 < \zeta, \\ 0 & \gamma_1 > \zeta. \end{cases} \quad (\text{B6})$$

Finally, we argue that an eigenstate exhibiting such a localization transition cannot exist for unit cell sizes $L = 1, 2$. First, if $L = 1$, then the system is completely translation-invariant for all $\gamma_1 \geq 0$. The OBC spectrum thus lies inside the area enclosed by the PBC spectral curve for all $\gamma_1 \geq 0$, in the sense that the winding number of the PBC curve about any OBC eigenenergy is always nonzero [67, 76]. For $L = 2$, both the PBC curve $E(k)$ and the OBC spectrum are symmetric about the imaginary line $-\frac{i\gamma_1}{4}$. This symmetry stems from the system being parity-time symmetric, up to translation by $\frac{i\gamma_1}{4}$ (note that the system also has a similar symmetry for $L = 1$, but not for $L > 2$). Therefore, such a purely imaginary OBC eigenenergy with $\text{Im } E_- < \text{Im } E(k)$ for all $k \in (-\pi, \pi)$ would be accompanied by another solution with $\text{Im } E_+ > \text{Im } E(k)$, which would be dynamically unstable, see Section V A. Since increasing $\gamma_1 \geq 0$ only creates more loss, it cannot spontaneously induce a dynamically unstable mode.

Appendix C: Susceptibility for the BKC with Two-Site Unit Cell

Using the equation of motion technique, we derive a closed form for the susceptibility of the system used in Section V A. Similarly to Appendix A, we start by deriving the susceptibility of a dissipative tight-binding model under OBC, here given by

$$\hat{H} = i\tilde{t} \sum_{j=1}^{N-1} \left(\hat{a}_{j+1}^\dagger \hat{a}_j - \hat{a}_j^\dagger \hat{a}_{j+1} \right) + \sum_{j=1}^N -\frac{i\gamma_j}{2} \hat{a}_j^\dagger \hat{a}_j \quad (\text{C1})$$

where $\gamma_j = \gamma_1 \geq 0$ when j is odd and $\gamma_j = \gamma_2 \geq 0$ when j is even. The retarded susceptibility is defined by

$$\tilde{\chi}(j, \ell; t) = \Theta(t) \langle [\hat{a}_j(t), \hat{a}_\ell^\dagger(0)] \rangle \quad (\text{C2})$$

and so

$$i\partial_t \tilde{\chi}(j, \ell; t) = i\delta(t)\delta_{j,\ell} + i\tilde{t}\tilde{\chi}(j-1, \ell; t) - i\tilde{t}\tilde{\chi}(j+1, \ell; t) - \frac{i\gamma_j}{2}\tilde{\chi}(j, \ell; t). \quad (\text{C3})$$

Taking the Fourier transform of $\tilde{\chi}$ with respect to t and denoting $\omega_j \equiv \omega + \frac{i\gamma_j}{2}$,

$$\omega_j \tilde{\chi}[j, \ell; \omega] = i\delta_{j,\ell} + i\tilde{t}\tilde{\chi}[j-1, \ell; \omega] - i\tilde{t}\tilde{\chi}[j+1, \ell; \omega]. \quad (\text{C4})$$

Up to some factor of i and with the boundary conditions $\tilde{\chi}[N+1, \ell; \omega] = 0$ and $\tilde{\chi}[0, \ell; \omega] = 0$, the source-free recurrence relation is that of the Chebyshev polynomial of the second kind U_j , which satisfies $U_{j+1}(x) =$

$2xU_j(x) - U_{j-1}(x)$ as well as $U_0(x) = 1$ and $U_1(x) = 2x$. The solution is readily found to be

$$\tilde{\chi}[j, \ell; \omega] = \frac{i^{j-\ell+1} U_{\min(j, \ell)-1}(\alpha) U_{N-\max(j, \ell)}(\alpha)}{\tilde{t} U_N(\alpha)} \rho_{j, \ell} \quad (\text{C5})$$

where $\alpha = \frac{\sqrt{\omega_1 \omega_2}}{2\tilde{t}}$ and

$$\rho_{j, \ell} = \sqrt{\frac{\omega_{\max(j, \ell)-1}}{\omega_{\min(j, \ell)}}}. \quad (\text{C6})$$

Repeating the same procedure outlined in Appendix A using Eq. (A3), we find that the average photon number is uniformly distributed between the unit cells at the critical value

$$\frac{\sqrt{\gamma_1 \gamma_2}}{2} = 2\Delta, \quad (\text{C7})$$

which corresponds precisely to the critical value separating the two topological phases that was found in Eq. (22). On the one hand, when $\frac{\sqrt{\gamma_1 \gamma_2}}{2} < 2\Delta$, the photons are exponentially localized on the last site of the chain. On the other hand, $\frac{\sqrt{\gamma_1 \gamma_2}}{2} > 2\Delta$ yields a photon distribution that is exponentially localized on the first site.

Appendix D: Line Gap Topology in Two-Site Unit Cell

Instead of having dissipation $-i\gamma_1/2$ and $-i\gamma_2/2$ on both sites of the two-site unit cell, suppose the first site experiences gain and the second site experiences loss. Balancing gain and loss, we have $\gamma_1 = -\gamma_2 = \gamma > 0$. In this case, the full Hamiltonian made up of $N/2$ unit cells is parity-time (PT) symmetric; it commutes with the operator PT , where P is the parity operator and T is responsible for time reversal [77]. Adapting the analysis given in the beginning of Section V A, we find that the dynamical block $M_x(k)$ only has one connected energy level when $\gamma/2 < 2t$ and has two when $\gamma/2 > 2t$. Accordingly, the critical value $\gamma/2 = 2t$ corresponds to the emergence of an imaginary line gap in the PBC spectrum. At the same time, the susceptibility of the system Eq. (C5) in steady state has

$$\tilde{\chi}[j, 1; 0] = \frac{i^j U_{N-j}(\frac{\gamma}{4t})}{\tilde{t} U_N(\frac{\gamma}{4t})} \sqrt{(-1)^j}. \quad (\text{D1})$$

Setting $x = \frac{\gamma}{4t}$ and $y = x + \sqrt{x^2 - 1}$, we find

$$U_n(x) = \frac{y^{n+1} - y^{-(n+1)}}{2\sqrt{x^2 - 1}}. \quad (\text{D2})$$

Since $|y| \geq 1$, we can drop the negative exponent terms when $N - j \gg 1$ such that

$$\tilde{\chi}[j, 1; 0] \simeq \frac{i^j \sqrt{(-1)^j}}{\tilde{t} y^j}. \quad (\text{D3})$$

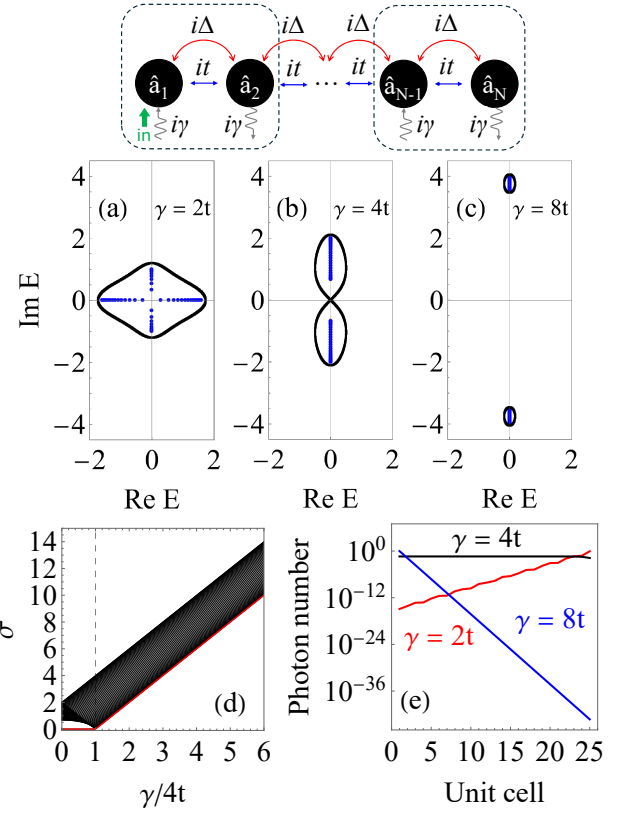


FIG. 8: (a)–(c) Spectrum, (d) singular values and (e) normalized steady-state unit cell photon number distribution for the two-site unit cell BKC with 50 sites (25 unit cells) and balanced gain and loss. In (a)–(c), the PBC (black) and OBC (blue) spectrum of M_x are shown for different coupling constants γ . There is a topological phase transition at $\gamma = 4t$. (d) Singular values of M_x for the open BKC as a function of γ . The critical dashed line $\gamma = 4t$ separates a regime wherein the smallest singular value (red) is exponentially small in system size from one in which it is not. In all plots $t = 1$ and $\Delta = 1/3$.

Using Eq. (A3), the photon number is again found to be given by Eq. (A10). However, since y is different here, the critical value $y_c = e^r$ is equivalent to $\gamma/2 = 2t$. That is, when $\gamma/2 < 2t$, the PBC system has one energy level and the photon number distribution is exponentially localized on the last site of the open chain. When $\gamma/2 > 2t$, the PBC spectrum corresponds to two disconnected loops and the photon number distribution is localized on the first site. Lastly, the photon number is uniformly distributed in the open chain at $\gamma/2 = 2t$. Thus, PT -symmetry makes the opening of the line gap topological. See Fig. 8.

Appendix E: Susceptibility for the BKC with Arbitrary Odd Bath Coupling Constants

We prove that the BKC of even length N exhibits exponential amplification independently of the values of odd bath coupling constants $\gamma_1, \gamma_3, \dots, \gamma_{N-1} \geq 0$, provided that $\gamma_2 = \gamma_4 = \dots = \gamma_N = 0$. To this end, we let $\tilde{\chi}$ denote the susceptibility of the dissipationless BKC given in Eq. (A5). Using Dyson's equation, we algebraically solve for the susceptibility $\tilde{\chi}_1$ of the system with dissipation on the first site, which corresponds to adding the term $(\tilde{V}_1)_{n,m} = -\frac{\gamma_1}{2}\delta_{n,1}\delta_{1,m}$ to the dynamical matrix. To incorporate dissipation on the third site, we add $(\tilde{V}_3)_{n,m} = -\frac{\gamma_3}{2}\delta_{n,3}\delta_{3,m}$ to the dynamical matrix and denote the associated susceptibility $\tilde{\chi}_3$. We repeat this procedure inductively until dissipation has been added on all odd sites, denoting by $\tilde{\chi}_{2j+1}$ the susceptibility of the system with $\tilde{V}_1, \tilde{V}_3, \dots, \tilde{V}_{2j+1}$. In the end, we prove by induction that $\tilde{\chi}_{N-1}[n, 1; \omega = 0] = \tilde{\chi}[n, 1; \omega = 0]$ for all $n = 1, \dots, N$. That is, the system's steady-state response on site n to a driving force on site 1 is independent of the fact that there is loss on the odd sites. We now proceed with the proof. First, note that the susceptibility of the dissipationless system given in Eq. (A5) has

$$\tilde{\chi}[n, 1; \omega = 0] = -\tilde{\chi}[1, n; \omega = 0] = \begin{cases} 0 & n \text{ odd,} \\ \tilde{t}^{-1} & n \text{ even} \end{cases} \quad (\text{E1})$$

as well as $\tilde{\chi}[\ell, \ell'; 0] = 0$ for any odd $1 \leq \ell, \ell' \leq N$. Adding \tilde{V}_1 to the dynamical matrix, Dyson's equation yields

$$\tilde{\chi}_1[n, m; \omega] = \tilde{\chi}[n, m; \omega] - \frac{\frac{\gamma_1}{2}\tilde{\chi}[n, 1; \omega]\tilde{\chi}[1, m; \omega]}{1 + \frac{\gamma_1}{2}\tilde{\chi}[1, 1; \omega]} \quad (\text{E2})$$

and in steady state ($\omega = 0$), we find

$$\tilde{\chi}_1[n, 1; 0] = -\tilde{\chi}_1[1, n; 0] = \tilde{\chi}[n, 1; 0]. \quad (\text{E3})$$

Additionally, $\tilde{\chi}_1[\ell, \ell'; 0] = 0$ for any odd $1 \leq \ell, \ell' \leq N$. Now, assume by induction that for some $j \geq 1$,

$$\tilde{\chi}_{2j-1}[n, 1; 0] = -\tilde{\chi}_{2j-1}[1, n; 0] = \tilde{\chi}[n, 1; 0] \quad (\text{E4})$$

as well as $\tilde{\chi}_{2j-1}[\ell, \ell'; 0] = 0$ for any odd $1 \leq \ell, \ell' \leq N$. Applying Dyson's equation for the next dissipative term \tilde{V}_{2j+1} , we readily obtain

$$\tilde{\chi}_{2j+1}[n, 1; 0] = -\tilde{\chi}_{2j+1}[1, n; 0] = \tilde{\chi}_{2j-1}[n, 1; 0] \quad (\text{E5})$$

and $\tilde{\chi}_{2j+1}[\ell, \ell'; 0] = 0$ for any odd $1 \leq \ell, \ell' \leq N$. By induction, the susceptibility $\tilde{\chi}_{N-1}$ of the even length BKC with arbitrary coupling constants $\gamma_1, \gamma_3, \dots, \gamma_{N-1} \geq 0$ on odd sites has $\tilde{\chi}_{N-1}[\ell, \ell'; 0] = 0$ for any odd $1 \leq \ell, \ell' \leq N$ as well as

$$\tilde{\chi}_{N-1}[n, 1; \omega = 0] = \tilde{\chi}[n, 1; \omega = 0] = \begin{cases} 0 & n \text{ odd,} \\ \tilde{t}^{-1} & n \text{ even.} \end{cases}$$

Using Eq. (A3), we conclude that the average photon number distribution is exponentially localized on the last site N , showing that system is in a non-trivial topological phase for arbitrary values of $\gamma_1, \gamma_3, \dots, \gamma_{N-1} \geq 0$.

-
- [1] S. Lieu, Topological symmetry classes for non-hermitian models and connections to the bosonic bogoliubov-de gennes equation, *Phys. Rev. B* **98**, 115135 (2018).
- [2] A. McDonald, T. Pereg-Barnea, and A. A. Clerk, Phase-dependent chiral transport and effective non-hermitian dynamics in a bosonic kitaev-majorana chain, *Phys. Rev. X* **8**, 041031 (2018).
- [3] Y.-X. Wang and A. A. Clerk, Non-hermitian dynamics without dissipation in quantum systems, *Phys. Rev. A* **99**, 063834 (2019).
- [4] V. P. Flynn, E. Cobanera, and L. Viola, Deconstructing effective non-hermitian dynamics in quadratic bosonic hamiltonians, *New Journal of Physics* **22**, 083004 (2020).
- [5] H. Katsura, N. Nagaosa, and P. A. Lee, Theory of the thermal hall effect in quantum magnets, *Phys. Rev. Lett.* **104**, 066403 (2010).
- [6] S. K. Kim, H. Ochoa, R. Zarzuela, and Y. Tserkovnyak, Realization of the haldane-kane-mele model in a system of localized spins, *Phys. Rev. Lett.* **117**, 227201 (2016).
- [7] D. F. Walls, Squeezed states of light, *Nature* **306**, 141 (1983).
- [8] C. M. Caves and B. L. Schumaker, New formalism for two-photon quantum optics. i. quadrature phases and squeezed states, *Phys. Rev. A* **31**, 3068 (1985).
- [9] C. M. Caves, Quantum-mechanical noise in an interferometer, *Phys. Rev. D* **23**, 1693 (1981).
- [10] J. Aasi et al., Enhanced sensitivity of the ligo gravitational wave detector by using squeezed states of light, *Nature Photonics* **7**, 613 (2013).
- [11] F. e. a. Acernese (Virgo Collaboration), Increasing the astrophysical reach of the advanced virgo detector via the application of squeezed vacuum states of light, *Phys. Rev. Lett.* **123**, 231108 (2019).
- [12] S. L. Braunstein and P. van Loock, Quantum information with continuous variables, *Rev. Mod. Phys.* **77**, 513 (2005).
- [13] J. Wiersig, Enhancing the sensitivity of frequency and energy splitting detection by using exceptional points: Application to microcavity sensors for single-particle detection, *Phys. Rev. Lett.* **112**, 203901 (2014).
- [14] J. Wiersig, Sensors operating at exceptional points: General theory, *Phys. Rev. A* **93**, 033809 (2016).
- [15] J. Wiersig, Review of exceptional point-based sensors, *Photon. Res.* **8**, 1457 (2020).
- [16] Z.-P. Liu, J. Zhang, i. m. c. K. Özdemir, B. Peng, H. Jing, X.-Y. Lü, C.-W. Li, L. Yang, F. Nori, and Y.-x. Liu,

- Metrology with \mathcal{PT} -symmetric cavities: Enhanced sensitivity near the \mathcal{PT} -phase transition, *Phys. Rev. Lett.* **117**, 110802 (2016).
- [17] H. Hodaei, A. U. Hassan, S. Wittek, H. Garcia-Gracia, R. El-Ganainy, D. N. Christodoulides, and M. Khajavikhan, Enhanced sensitivity at higher-order exceptional points, *Nature* **548**, 187 (2017).
- [18] W. Chen, Ş. Kaya Özdemir, G. Zhao, J. Wiersig, and L. Yang, Exceptional points enhance sensing in an optical microcavity, *Nature* **548**, 192 (2017).
- [19] M. Zhang, W. Sweeney, C. W. Hsu, L. Yang, A. D. Stone, and L. Jiang, Quantum noise theory of exceptional point amplifying sensors, *Phys. Rev. Lett.* **123**, 180501 (2019).
- [20] R. El-Ganainy, K. G. Makris, M. Khajavikhan, Z. H. Musslimani, S. Rotter, and D. N. Christodoulides, Non-hermitian physics and pt symmetry, *Nature Physics* **14**, 11 (2018).
- [21] J. Ren, H. Hodaei, G. Harari, A. U. Hassan, W. Chow, M. Soltani, D. Christodoulides, and M. Khajavikhan, Ultrasensitive micro-scale parity-time-symmetric ring laser gyroscope, *Opt. Lett.* **42**, 1556 (2017).
- [22] Y.-Y. Wang, C.-W. Wu, W. Wu, and P.-X. Chen, \mathcal{PT} -symmetric quantum sensing: Advantages and restrictions, *Phys. Rev. A* **109**, 062611 (2024).
- [23] X.-W. Luo, C. Zhang, and S. Du, Quantum squeezing and sensing with pseudo-anti-parity-time symmetry, *Phys. Rev. Lett.* **128**, 173602 (2022).
- [24] Y.-H. Lai, Y.-K. Lu, M.-G. Suh, Z. Yuan, and K. Vahala, Observation of the exceptional-point-enhanced sagnac effect, *Nature* **576**, 65 (2019).
- [25] S. Yao and Z. Wang, Edge states and topological invariants of non-hermitian systems, *Phys. Rev. Lett.* **121**, 086803 (2018).
- [26] V. M. Martinez Alvarez, J. E. Barrios Vargas, and L. E. F. Foa Torres, Non-hermitian robust edge states in one dimension: Anomalous localization and eigenspace condensation at exceptional points, *Phys. Rev. B* **97**, 121401 (2018).
- [27] J. C. Budich and E. J. Bergholtz, Non-hermitian topological sensors, *Phys. Rev. Lett.* **125**, 180403 (2020).
- [28] C. Ehrhardt and J. Larson, Exploring the impact of fluctuation-induced criticality on non-hermitian skin effect and quantum sensors, *Phys. Rev. Res.* **6**, 023135 (2024).
- [29] S. Sarkar, F. Ciccarello, A. Carollo, and A. Bayat, Critical non-hermitian topology induced quantum sensing, *New Journal of Physics* **26**, 073010 (2024).
- [30] L. Bao, B. Qi, and D. Dong, Exponentially enhanced quantum non-hermitian sensing via optimized coherent drive, *Phys. Rev. Appl.* **17**, 014034 (2022).
- [31] A. McDonald and A. A. Clerk, Exponentially-enhanced quantum sensing with non-hermitian lattice dynamics, *Nature Communications* **11**, 5382 (2020).
- [32] L. Deák and T. Fülöp, Reciprocity in quantum, electromagnetic and other wave scattering, *Annals of Physics* **327**, 1050 (2012).
- [33] C. Caloz, A. Alù, S. Tretyakov, D. Sounas, K. Achouri, and Z.-L. Deck-Léger, Electromagnetic nonreciprocity, *Phys. Rev. Appl.* **10**, 047001 (2018).
- [34] H.-K. Lau and A. A. Clerk, Fundamental limits and non-reciprocal approaches in non-hermitian quantum sensing, *Nature Communications* **9**, 4320 (2018).
- [35] A. Metelmann and A. A. Clerk, Nonreciprocal photon transmission and amplification via reservoir engineering, *Phys. Rev. X* **5**, 021025 (2015).
- [36] A. Metelmann and A. A. Clerk, Nonreciprocal quantum interactions and devices via autonomous feedforward, *Phys. Rev. A* **95**, 013837 (2017).
- [37] K. Fang, J. Luo, A. Metelmann, M. H. Matheny, F. Marquardt, A. A. Clerk, and O. Painter, Generalized non-reciprocity in an optomechanical circuit via synthetic magnetism and reservoir engineering, *Nature Physics* **13**, 465 (2017).
- [38] A. Kamal, J. Clarke, and M. H. Devoret, Noiseless non-reciprocity in a parametric active device, *Nature Physics* **7**, 311 (2011).
- [39] B. Abdo, K. Sliwa, L. Frunzio, and M. Devoret, Directional amplification with a josephson circuit, *Phys. Rev. X* **3**, 031001 (2013).
- [40] K. M. Sliwa, M. Hatridge, A. Narla, S. Shankar, L. Frunzio, R. J. Schoelkopf, and M. H. Devoret, Reconfigurable josephson circulator/directional amplifier, *Phys. Rev. X* **5**, 041020 (2015).
- [41] D. Malz, L. D. Tóth, N. R. Bernier, A. K. Feofanov, T. J. Kippenberg, and A. Nunnenkamp, Quantum-limited directional amplifiers with optomechanics, *Phys. Rev. Lett.* **120**, 023601 (2018).
- [42] Z. Shen, Y.-L. Zhang, Y. Chen, C.-L. Zou, Y.-F. Xiao, X.-B. Zou, F.-W. Sun, G.-C. Guo, and C.-H. Dong, Experimental realization of optomechanically induced non-reciprocity, *Nature Photonics* **10**, 657 (2016).
- [43] F. Ruesink, M.-A. Miri, A. Alù, and E. Verhagen, Non-reciprocity and magnetic-free isolation based on optomechanical interactions, *Nature Communications* **7**, 13662 (2016).
- [44] X.-W. Xu, Y. Li, A.-X. Chen, and Y.-x. Liu, Nonreciprocal conversion between microwave and optical photons in electro-optomechanical systems, *Phys. Rev. A* **93**, 023827 (2016).
- [45] N. R. Bernier, L. D. Tóth, A. Koottandavida, M. A. Ioannou, D. Malz, A. Nunnenkamp, A. K. Feofanov, and T. J. Kippenberg, Nonreciprocal reconfigurable microwave optomechanical circuit, *Nature Communications* **8**, 604 (2017).
- [46] G. A. Peterson, F. Lecocq, K. Cicak, R. W. Simmonds, J. Aumentado, and J. D. Teufel, Demonstration of efficient nonreciprocity in a microwave optomechanical circuit, *Phys. Rev. X* **7**, 031001 (2017).
- [47] A. Y. Kitaev, Unpaired majorana fermions in quantum wires, *Physics-Uspekhi* **44**, 131–136 (2001).
- [48] J. J. Slim, C. C. Wanjura, M. Brunelli, J. del Pino, A. Nunnenkamp, and E. Verhagen, Optomechanical realization of the bosonic kitaev chain, *Nature* **627**, 767 (2024).
- [49] J. H. Busnaina, Z. Shi, A. McDonald, D. Dubyna, I. Nsanzineza, J. S. C. Hung, C. W. S. Chang, A. A. Clerk, and C. M. Wilson, Quantum simulation of the bosonic kitaev chain, *Nature Communications* **15**, 3065 (2024).
- [50] C. C. Wanjura, M. Brunelli, and A. Nunnenkamp, Topological framework for directional amplification in driven-dissipative cavity arrays, *Nature Communications* **11**, 3149 (2020).
- [51] D. Porras and S. Fernández-Lorenzo, Topological amplification in photonic lattices, *Phys. Rev. Lett.* **122**, 143901 (2019).

- [52] M. Brunelli, C. C. Wanjura, and A. Nunnenkamp, Restoration of the non-Hermitian bulk-boundary correspondence via topological amplification, *SciPost Phys.* **15**, 173 (2023).
- [53] L. Herviou, J. H. Bardarson, and N. Regnault, Defining a bulk-edge correspondence for non-hermitian hamiltonians via singular-value decomposition, *Phys. Rev. A* **99**, 052118 (2019).
- [54] F. Cardano, A. D'Errico, A. Dauphin, M. Maffei, B. Piccirillo, C. de Lisis, G. De Filippis, V. Cataudella, E. Santamato, L. Marrucci, M. Lewenstein, and P. Massignan, Detection of zak phases and topological invariants in a chiral quantum walk of twisted photons, *Nature Communications* **8**, 15516 (2017).
- [55] M. Maffei, A. Dauphin, F. Cardano, M. Lewenstein, and P. Massignan, Topological characterization of chiral models through their long time dynamics, *New Journal of Physics* **20**, 013023 (2018).
- [56] S. Longhi, Probing one-dimensional topological phases in waveguide lattices with broken chiral symmetry, *Opt. Lett.* **43**, 4639 (2018).
- [57] Z.-Q. Jiao, S. Longhi, X.-W. Wang, J. Gao, W.-H. Zhou, Y. Wang, Y.-X. Fu, L. Wang, R.-J. Ren, L.-F. Qiao, and X.-M. Jin, Experimentally detecting quantized zak phases without chiral symmetry in photonic lattices, *Phys. Rev. Lett.* **127**, 147401 (2021).
- [58] G. Cáceres-Aravena, B. Real, D. Guzmán-Silva, P. Vildoso, I. Salinas, A. Amo, T. Ozawa, and R. A. Vicencio, Edge-to-edge topological spectral transfer in diamond photonic lattices, *APL Photonics* **8**, 080801 (2023).
- [59] G. Villa, I. Carusotto, and T. Ozawa, Mean-chiral displacement in coherently driven photonic lattices and its application to synthetic frequency dimensions, *Communications Physics* **7**, 246 (2024).
- [60] C. C. Wanjura, M. Brunelli, and A. Nunnenkamp, Correspondence between non-hermitian topology and directional amplification in the presence of disorder, *Phys. Rev. Lett.* **127**, 213601 (2021).
- [61] T. Ramos, J. J. García-Ripoll, and D. Porras, Topological input-output theory for directional amplification, *Phys. Rev. A* **103**, 033513 (2021).
- [62] A. Gómez-León, T. Ramos, A. González-Tudela, and D. Porras, Bridging the gap between topological non-hermitian physics and open quantum systems, *Phys. Rev. A* **106**, L011501 (2022).
- [63] A. A. Clerk, M. H. Devoret, S. M. Girvin, F. Marquardt, and R. J. Schoelkopf, Introduction to quantum noise, measurement, and amplification, *Rev. Mod. Phys.* **82**, 1155 (2010).
- [64] A. Altland and M. R. Zirnbauer, Nonstandard symmetry classes in mesoscopic normal-superconducting hybrid structures, *Phys. Rev. B* **55**, 1142 (1997).
- [65] K. Kawabata, K. Shiozaki, M. Ueda, and M. Sato, Symmetry and topology in non-hermitian physics, *Phys. Rev. X* **9**, 041015 (2019).
- [66] This differs from the class AIII[†] identified in [49] since we choose the hopping and parametric coupling to be imaginary, allowing for the additional particle-hole type symmetry PHS[†] [65] given by $-\hat{H}^* = \hat{H}$. Nonetheless, both classes have the same \mathbb{Z}_2 topological invariant in 1D, see [49].
- [67] N. Okuma, K. Kawabata, K. Shiozaki, and M. Sato, Topological origin of non-hermitian skin effects, *Phys. Rev. Lett.* **124**, 086801 (2020).
- [68] K. Zhang, Z. Yang, and C. Fang, Correspondence between winding numbers and skin modes in non-hermitian systems, *Phys. Rev. Lett.* **125**, 126402 (2020).
- [69] C. H. Lee and R. Thomale, Anatomy of skin modes and topology in non-hermitian systems, *Phys. Rev. B* **99**, 201103 (2019).
- [70] Z. Gong, Y. Ashida, K. Kawabata, K. Takasan, S. Higashikawa, and M. Ueda, Topological phases of non-hermitian systems, *Phys. Rev. X* **8**, 031079 (2018).
- [71] D. S. Borgnia, A. J. Kruchkov, and R.-J. Slager, Non-hermitian boundary modes and topology, *Phys. Rev. Lett.* **124**, 056802 (2020).
- [72] N. Hatano and D. R. Nelson, Localization transitions in non-hermitian quantum mechanics, *Phys. Rev. Lett.* **77**, 570 (1996).
- [73] N. Hatano and D. R. Nelson, Vortex pinning and non-hermitian quantum mechanics, *Phys. Rev. B* **56**, 8651 (1997).
- [74] Although this seems to come from our choice of gauge, the PHS[†] property of Eq. (20) is gauge independent. One can readily derive $M = -M^*$ for the full dynamical matrix from the dynamical equation in the quadrature basis, as \hat{x}_j and \hat{p}_j are Hermitian operators. However, depending on the gauge $\hat{a}_j \rightarrow e^{i\theta_j} \hat{a}_j$, M might not be block diagonal in the usual quadrature basis $\hat{x}_j = \frac{1}{2}(\hat{a}_j + \hat{a}_j^\dagger)$ and $\hat{p}_j = \frac{1}{2i}(\hat{a}_j - \hat{a}_j^\dagger)$. Instead, the block diagonal basis is $\hat{x}_j = \frac{e^{i\theta}}{2}(\hat{a}_j + e^{-2i\theta_j} \hat{a}_j^\dagger)$ and $\hat{p}_j = \frac{e^{i\theta}}{2i}(\hat{a}_j - e^{-2i\theta_j} \hat{a}_j^\dagger)$.
- [75] S. Gerschgorin, Über die abgrenzung der eigenwerte einer matrix, *Izv. Akad. Nauk. SSSR. Otd. Fiz.-Mat. Nauk* **7**, 749 (1931).
- [76] N. Okuma and M. Sato, Non-hermitian topological phenomena: A review, *Annual Review of Condensed Matter Physics* **14**, 83 (2023).
- [77] C. M. Bender and S. Boettcher, Real spectra in non-hermitian hamiltonians having \mathcal{PT} symmetry, *Phys. Rev. Lett.* **80**, 5243 (1998).